Proceedings of the 11th ICPMG 2026
11th International Conference on Physical Modelling in Geotechnics
8-12 June 2026, Zurich, Switzerland

Development of a climate-controlled chamber: measurement and characterization of the clay response

Mohd Sheob
University of Colorado, Boulder, USA, mohd.sheob@colorado.edu

Sarah Aldawood, Srikanth S. C. Madabhushi
University of Colorado, Boulder, USA, sarah.aldawood@colorado.edu, mscs@colorado.edu

ABSTRACT: Changes in average ambient temperature and relative humidity can impact the stability of geostructures such as slopes and earth retaining systems. The sensitivity of these systems to such changes depends on the soil response which often can be difficult to measure and characterize. This study presents the design and development of a new climate-controlled chamber at the University of Colorado Boulder. The performance of the closed-loop control systems is first discussed. Following this, the measurement and interpretation of the soil response are presented. Attention is paid to the instrumentation of the soil during the model preparation (e.g., from a slurry to a consolidated deposit using a hydraulic press) through to the observed response to controlled changes in the ambient conditions. Direct and inferred measurements of the pore pressures, temperature, shear strength, relative humidity, and water content are considered. The instrumentation setup demonstrates how complex thermo-hydro-mechanical responses of fine-grained soils can be measured and linked to the ambient conditions, laying the groundwork for future centrifuge studies investigating the stability of geostructures in changing environments.

1 INTRODUCTION

Climate change is leading to sustained increases in average ambient temperature and altered atmospheric moisture conditions, which can significantly influence the performance and stability of geotechnical systems such as slopes, embankments, and earth-retaining structures (Archer & Ng, 2018; Moncada et al., 2024; Ng et al., 2024; Pritchard et al., 2014; Wang et al., 2025). Of these factors, fluctuations in temperature and relative humidity (RH) can play a dominant role (François & Laloui, 2008). Fine-grained soils, particularly clays, are known to exhibit strong thermo-hydro-mechanical coupling, where changes in temperature and boundary RH induce variations in pore water pressure, soil fabric, strains, shear strength, and the elasto-plastic response of the soil (Archer & Ng, 2018; Hueckel & Borsetto, 1990; Robinet et al., 1996; Shibasaki et al., 2017). Nevertheless, experimental characterization of the soil response under controlled thermal and atmospheric conditions remains limited, particularly at the scale of models relevant to centrifuge testing.

Previous efforts to control the climate in centrifuge containers have provided valuable insights into soil–atmosphere interactions. However, in many cases, either the temperature or RH was not controlled or could not be varied independently; in others, the achievable RH range was limited e.g., typically between 55–88% (Castiblanco et al., 2016; Hudacsek et al., 2009; Matziaris et al., 2015; Take & Bolton, 2002; Tristancho et al., 2012). The current study presents the design, development, and performance evaluation of a climate-controlled experimental chamber capable of independently regulating temperature and RH above a saturated clay specimen. This study is part of a larger effort to link THM mechanisms observed at the element scale to macroscale slope failures.

The system developed is conceived to be compatible with future centrifuge testing at the University of Colorado Boulder, enabling detailed monitoring of soil response during sample preparation, consolidation, and thermal loading. A series of closed-loop proportional–integral–derivative (PID) control schemes are implemented and systematically tuned to achieve stable and repeatable environmental conditions. Using Speswhite Kaolin clay, the study investigates the thermo-mechanical response of a saturated fine-grained soil subjected to controlled heating and cooling cycles. Undrained shear strength is quantified using miniature T-bar penetration tests, while internal soil processes are monitored through embedded temperature sensors and pore pressure transducers. By integrating environmental control with direct and inferred measurements of the soil response, this work provides insight into studying thermally induced strength changes in clays and establishes a foundation for future physical modelling investigations into climate-driven geostructural instabilities.

2 METHODOLOGY

All experiments were conducted in a rigid centrifuge container that was modified to enable controlled thermal and RH loading while maintaining well-defined mechanical boundary conditions. The testing procedure comprised of two sequential phases. In the first phase, the soil specimen was subjected to one-dimensional consolidation at ambient laboratory condition to establish a uniform stress state and reproducible initial conditions. In the second phase, the thermomechanical response of the clay was characterized at different imposed temperatures through a series of T-bar penetration tests, while a constant RH of the atmosphere and water content of the soil was targeted.

2.1 Material and sample preparation

The soil used in this study is Speswhite Kaolin; a commercially available fine-grained clay that has previously been shown to exhibit thermal sensitivity (Sheob & Madabhushi, 2026). The index properties of the Kaolin clay include a plastic limit of 38%, a liquid limit of 69%, and specific gravity of 2.61 (Cao et al., 2002). To prepare the soil deposit, dry Kaolin powder was mixed with water to achieve a water content of 140%, corresponding to approximately twice the liquid limit of the soil. This elevated water content was selected to both promote a homogenous slurry and encourage a thermally sensitive fabric. Mixing was performed using a vacuum mixer with a total capacity of 169,901 cm^3 (6 ft^3), which minimized air entrapment of the prepared slurry.

2.2 Experiment container and thermal control

The slurry was poured into the modified centrifuge container, herein referred to as the Environmental Control Test Box (ECTB), with internal dimensions of 90.5 cm (length) × 34.5 cm (width) × 34 cm (height). The front wall of the box was made of transparent material to facilitate Digital Image Correlation in future experiments. To enable controlled thermal loading while protecting the insulation material, three vertical sides of the box (excluding the front wall) and the base were lined with a 0.635 cm thick high temperature-resistant Ultra-High Molecular Weight (UHMW) polyethylene sheet. Routed grooves were incorporated into the UHMW sheets to accommodate heating cables. Behind the UHMW polyethylene, a 1.905 cm thick layer of Expanded Polystyrene Sheet (EPS) insulation was installed on the same three sides and base of the box. Prior to installation of the UHMW polyethylene and EPS layers, filter paper with a pore size smaller than 5 µm was placed along the base of the box to retain soil particles. This arrangement enabled a double drainage condition during consolidation, i.e., allowing excess pore dissipation both upwards and downwards. This configuration effectively reduces heat loss and the layout of the experimental setup is shown in Figure 1 (Sheob et al., 2026). Temperature regulation was achieved using a PID feedback control system.

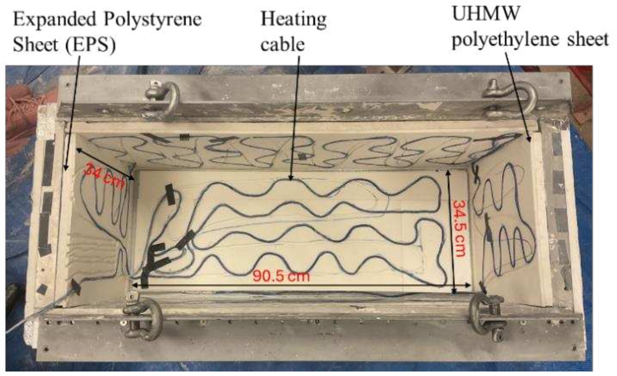

Figure 1. Insulation and heating within the environmental control test box.

2.3 Sample Placement and Instrumentation

The kaolin slurry was placed in two layers. After placement of the first layer of slurry it was consoldiated in the hydraulic press. Thermistor-type temperature sensors, pore pressure transducers (PPTs), and TEROS 12 probes were then embedded at predefined locations (Figure 2) to monitor temperature, pore water pressure, and water content throughout the experiment. However, PPT-1 and PPT-2 failed during consolidation and the TEROS 12 data is not discussed in this study pending calibrations accounting for thermal sensitivity. A second slurry layer was subsequently placed over the instrumented first layer and further consolidated to achieve the final soil state and thickness described in the following section.

2.4 Consolidation procedure

Consolidation was performed using a 50-ton hydraulic press at the Center for Infrastructure, Energy and Space Testing (CIEST), University of Colorado Boulder. A controlled consolidation program was conducted using a piston displacement rate of 0.4572 cm/hour which was maintained until a total stress of 200 kPa was reached, based on deformation-based termination criteria. Consolidation continued until the vertical strain rate of the soil specimen reduced to less than 0.005% per minute over the preceding one-hour interval. This procedure ensured that primary consolidation was effectively complete before proceeding with subsequent experimental stages. Figure 3 shows the evolution of total stress, effective stress, and pore water pressure, along with displacement, during consolidation of the second layer.

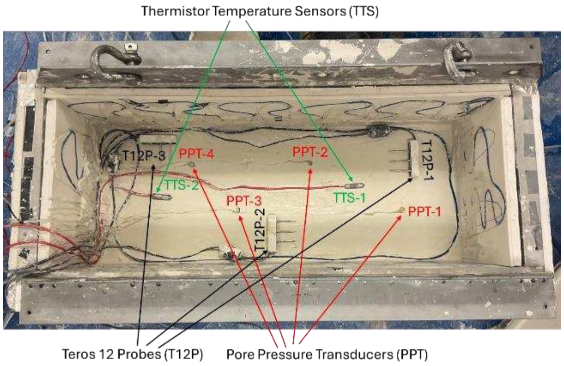

(a)

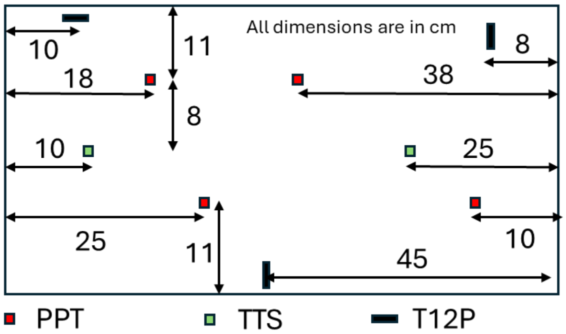

(b)

Figure 2. (a) Sensor layout after first-layer consolidation (b) Overall locations of all installed sensors.

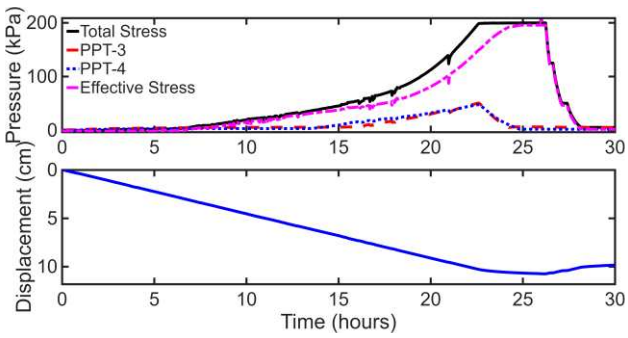

Figure 3. Illustrative total stress, pore pressure, and effective stress evolution and piston displacement during consolidation of the second layer.

Table 1. Summarize the specimen conditions following consolidation of both layers.

Layer index	Initial height (cm)	Final height (cm)	Water content (%)	Void ratio
I	17	6.39	53.2	1.38
II	17.4	7.08	54.5	1.42

* Initial heights correspond to slurry height while final height and other state parameters represent the post-consolidation condition of each layer, assuming full saturation ($s_r = 1$)

2.5 Lid assembly and relative humidity Control

Following completion of consolidation, a prototype of a Relative Humidity Control Lid (RHCL) was placed over the ECTB to regulate the RH boundary conditions above the soil surface. The prototype was fabricated from wood for expediency and is not intended for a centrifuge environment. The RHCL incorporates two brushless fans mounted on its underside and oriented in opposite directions to promote uniform air circulation within the enclosed headspace and to facilitate exchange between the RHCL volume and the soil surface. To generate humid air, two mini mist makers are installed in a water container and connected to the RHCL enclosure, as illustrated in Figure 4a where the top plate of the RHCL is removed. This system enabled controlled humidification of the air above the soil specimen. The RH within the box was controlled using a PID feedback control system. Two RH sensors (RHS) were suspended from the underside of the RHCL and positioned to directly face the soil surface, shown schematically in Figure 4b. The successful performance of this RHCL is intended as a proof of concept, with the long-term objective of adapting the design for a hyper-gravity environment.

Prior to placement of the RHCL, a shallow pool of water was introduced over the soil surface. This measure was implemented to minimize moisture loss due to evaporation during thermal loading. By maintaining a saturated surface boundary condition, changes in the mechanical response of the soil at depth can be attributed primarily to thermal effects rather than to water loss or suction-induced stiffening. This approach ensures that the observed soil behavior during heating was isolated from coupled thermo-hydraulic drying effects. As the clay is fully saturated it is not expected to swell significantly to absorb this water, though with time the surface of clay particles may disperse into the pool leading to a locally weakened, slurry-like surface. Once the RHCL was placed over the box, the heating and RH cycles were initiated to achieve the prescribed target temperature and RH conditions.

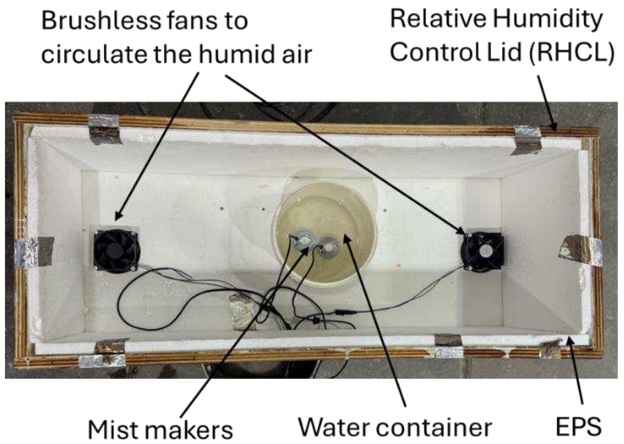

(a)

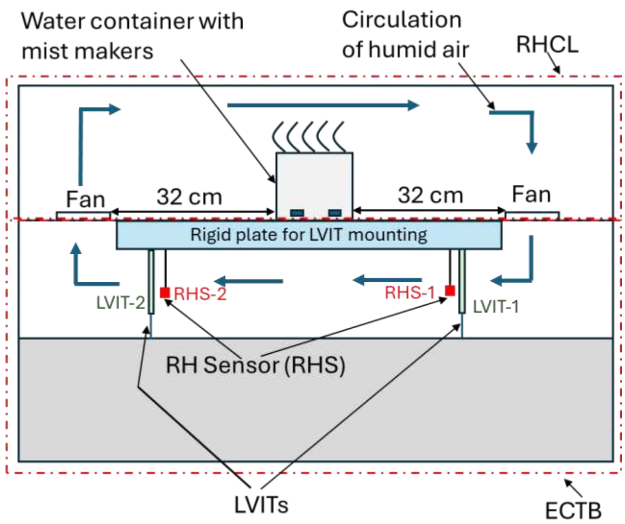

(b)

Figure 4. (a) Relative himidty control lid configuration (b) Schematic diagram of RHLC with ECTB.

2.6 T-bar configuration

After achieving the target temperature and RH conditions, the RHCL was carefully removed to expose the soil surface to ambient conditions, and a miniature T-bar penetrometer (White et al., 2010) was then used to determine the undrained shear strength (s_u) profile of the soil. The T-bar was guided vertically into the soil using the hydraulic press, with the reaction force and penetration displacement recorded using a load cell and a string potentiometer respectively, as shown in Figure 5. For each test, the T-bar was penetrated to a depth of 7 cm at three new locations within the specimen. The average resistive force from these measurements was used for subsequent analysis. The T-bar geometry consisted of a cylindrical shaft with a bottom diameter of 0.636 cm and a length of 5 cm. The undrained shear strength, s_u, was computed using the standard relation in equation 1:

$$s_u = {}^{q}/_{N_T} \qquad (1)$$

where q is the measured resistive force per unit projected area, and N_T is a bearing capacity factor that reflects the stress distribution and/or failure mechanism around the T-bar. A value of $N_T = 10.5$ was adopted in this study (Stewart & Randolph, 1991) and is assumed constant for all temperatures.

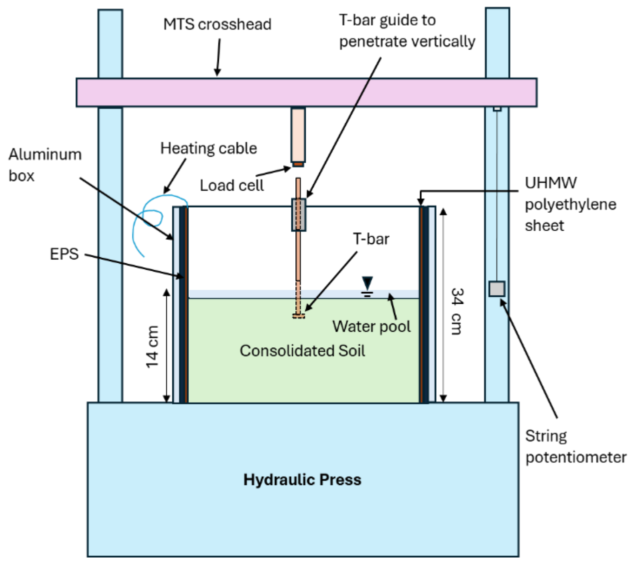

(a)

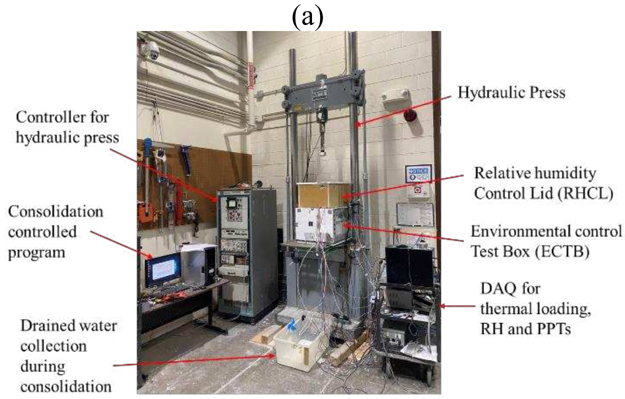

(b)

Figure 5. Experimental setup (a) Overall schematic diagram (b) Photograph of experimental setup

3 RESULTS

The experimental results are presented in terms of (i) target temperature control by the ECTB, (ii) Control performance with the RHCL, and (iii) the thermo-mechanical response of the clay specimen.

3.1 Temperature control performance

Temperature regulation was implemented using a PID feedback controller calibrated through preliminary tuning tests. The controller was first operated with the integral and derivative gains set to zero ($k_i = 0$, $k_d = 0$), while the proportional gain was varied ($k_p = 0.5, 1,$ and 2) during heating–cooling cycles between 25 °C and 17 °C. As shown in Figure 6a, $k_p = 2$ provided the best convergence to the target temperature, with reduced steady-state error and acceptable undershoot, and was therefore selected. Subsequently, with $k_p = 2$ and $k_d = 0$, the integral gain was varied ($k_i = 0.5$ and 1) during thermal cycling between 22 °C and 18 °C (Figure 6b). Although the inclusion of an integral term improved tracking accuracy, $k_i = 0.5$ caused increased overshoot and slower stabilization, whereas $k_i = 1$ achieved stable regulation with minimal steady-state offset and was adopted.

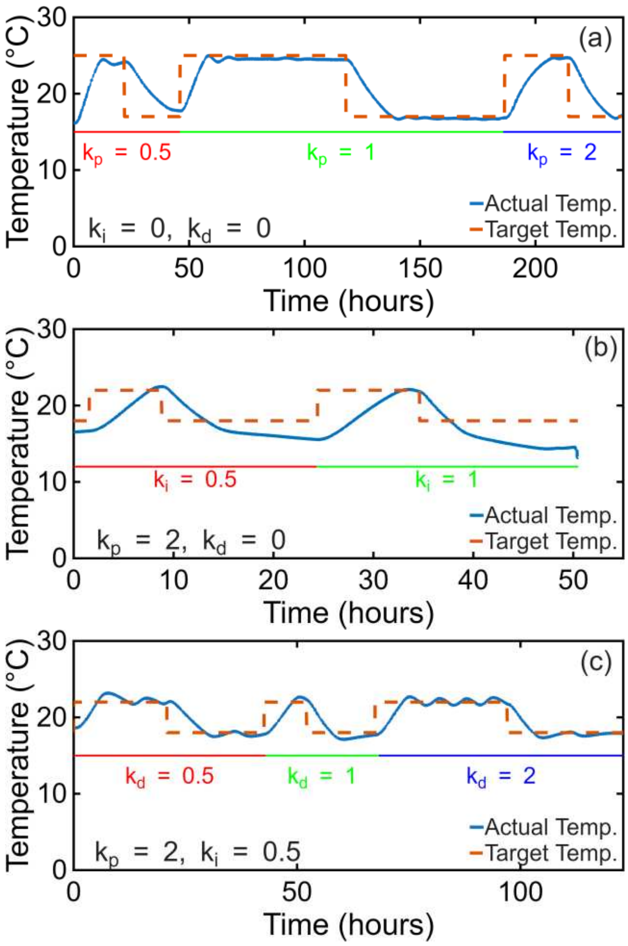

Figure 6. Temperature control performance of the environmental control test box during PID tuning.

Finally, with $k_p = 2$ and $k_i = 1$ fixed, the derivative gain was varied ($k_d = 0.5, 1,$ and 2) under the same heating–cooling range (Figure 6c). Increasing k_d enhanced damping and reduced oscillations, with $k_d = 2$ yielding the smoothest and most stable response. Consequently, the final controller parameters adopted were $k_p = 2$, $k_i = 1$, and $k_d = 2$.

3.2 Relative humidity control performance

The RH was controlled using the same PID framework as the temperature control. Initial tuning was conducted by varying the proportional gain with $k_i = 0$ and $k_d = 0$, testing $k_p = 0.25, 0.5, 1,$ and 1.25. The lowest gain ($k_p = 0.25$) produced a sluggish response, whereas $k_p = 0.5, 1,$ and 1.25 showed similarly stable performance with comparable rise times (Figure 7a). Consequently, $k_p = 1$ was selected for subsequent tuning. With k_p fixed, the integral and derivative gains were varied individually ($k_i, k_d = 0.25$ and 0.5) while setting the remaining gain to zero (Figure 7b). Increasing k_i caused a delayed RH response,

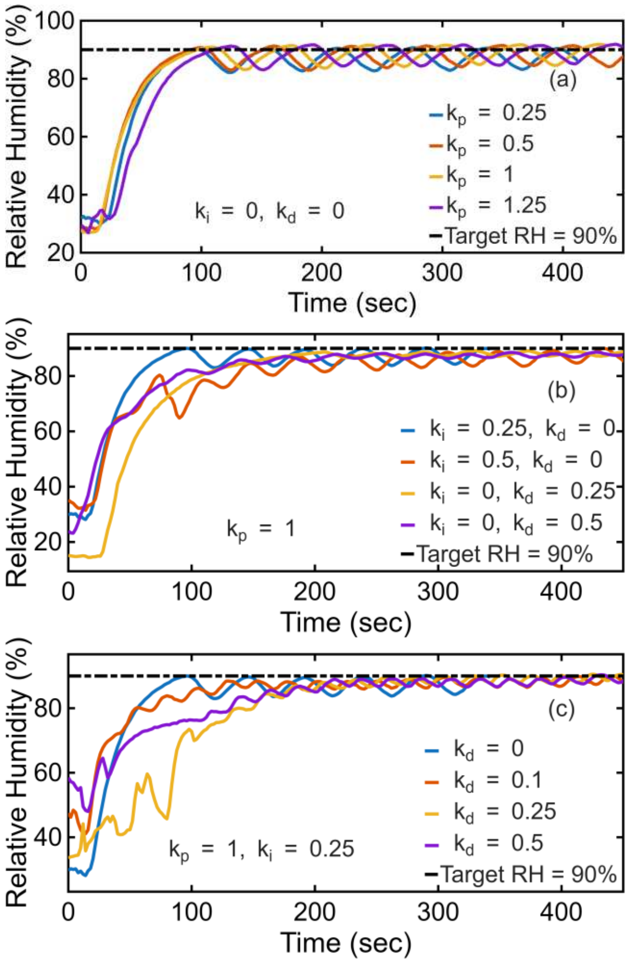

Figure 7. RH control performance of the environmental control test box during PID tuning.

pronounced undershoot, and longer settling times. This indicates excessive error accumulation during transients. Similarly, increasing k_d with $k_i = 0$ led to persistent undershoot and failure to reach the target RH. Consequently, $k_i = 0.25$ was selected as a compromise between response speed and stability, and subsequent tuning of k_d was conducted using this value (Figure 7c). Finally, with $k_p = 1$ and $k_i = 0.25$ fixed, the derivative gain was evaluated and found to introduce delays without improving stability or reducing undershoot. Accordingly, the derivative term was omitted. The final parameters selected for RH control were $k_p = 1$, $k_i = 0.25$, and $k_d = 0$, which provided the most stable and responsive performance and were used in all subsequent experiments.

3.3 Thermomechanical response of the soil

The thermomechanical response of the clay was evaluated in terms of pore water pressure, soil displacement, and undrained shear strength (s_u) during controlled heating and cooling cycles. The temperature was increased from room temperature (24 °C) to 35 °C and further to 45 °C (Figure 8), while the RH within the ECTB was targeted at 80%. Although RH effects were not investigated explicitly, the ECTB demonstrated sufficient capability to regulate RH; however, continuous humidification required periodic refilling of the water container supplying the mist makers. Once the container became empty, a gradual reduction in RH was observed within the box. Ideally, RH should remain constant even after water depletion; however, the prototype RHCL was likely not fully sealed, allowing moisture exchange with the very low ambient laboratory RH.

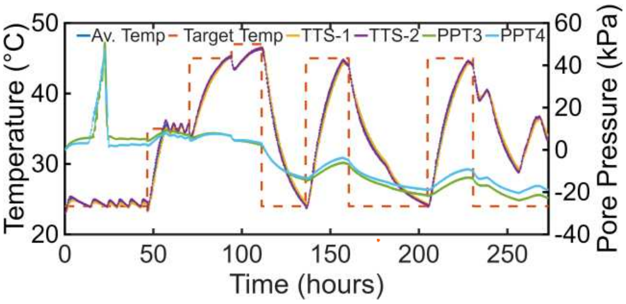

Figure 8. Response of pore water pressure under heating–cooling cycles.

Figure 8 presents the pore water pressure response during consolidation and thermal cycling. Consolidation of the second soil layer generated excess pore pressure that dissipated within approximately two hours, indicating near-complete primary consolidation, although the PPTs could not reliably capture suction after unloading. During the first heating cycle, pore pressure increased markedly, consistent with thermal pressurization under undrained conditions. Partial dissipation was observed once the temperature stabilized at 35 °C, suggesting limited drainage and/or redistribution of pore pressures. In subsequent cycles, isothermal periods were short due to immediate T-bar testing. Consequently, it is difficult to conclusively assess whether pore pressure would consistently dissipate under prolonged isothermal conditions.

Despite these limitations, pore pressure closely followed the imposed thermal cycles, increasing during heating and decreasing during cooling. During cooling, pore pressure reductions exceeded heating-induced increases, suggesting suction development and a thermo-hydraulic coupling in the saturated clay. Figure 9a shows the evolution of RH during the test. Overall, RH was maintained close to the target value for most of the experimental duration. Short-term reductions in RH occurred intermittently, primarily due to limitations of the mist makers. As the water level in the reservoir decreased, mist production reduced, while at higher water heads the mist makers occasionally ceased operation, leading to brief RH fluctuations. Additionally, after each target temperature was reached, the RHCL was removed to perform T-bar penetration tests, causing a rapid drop in RH. Upon re-placing the RHCL and initiating the next thermal stage, RH recovered quickly and returned to the target value, demonstrating the responsiveness of the control system.

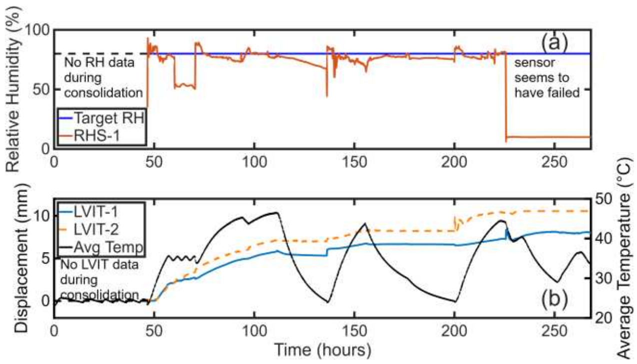

Figure 9. (a) Relative humidity response (b) settlement response during heating–cooling cycles.

Figure 9b illustrates the LVIT-measured vertical displacement together with the average temperature. A pronounced volumetric expansion was observed during the first heating stage, whereas the subsequent cooling phase resulted in negligible contraction. This asymmetric response is attributed to the saturation condition maintained prior to heating, during which an additional water pool was introduced. The absorbed water increased the soil water content, as evidenced in Figure 10 and discussed in a later subsection. Consequently, the extensive expansion observed during first heating is interpreted as the combined effect of thermal expansion and water uptake by the soil. Reheating again induced volumetric expansion, albeit with a reduced magnitude compared to the first heating stage. This response is consistent with the observed pore pressure evolution: heating-induced expansion reflects thermal pressurization under predominantly undrained conditions, whereas the limited contraction during cooling indicates partial dissipation of excess pore pressure. The attenuated expansion during reheating suggests partial irreversibility of the deformation process and progressive thermomechanical softening of the clay.

Figure 10 presents the traditional gravimetric water content (GWC) measured at the soil surface and at a depth of 7 cm following consolidation and subsequent thermal cycling. The post-consolidation water contents were lower than those measured during thermal cycling due to the intentional addition of a shallow surface water layer to maintain saturation and minimize evaporation. As a result, the water content remained approximately constant during subsequent heating and cooling phases, indicating that the observed variations in undrained shear strength were predominantly thermally induced rather than driven by changes in moisture content.

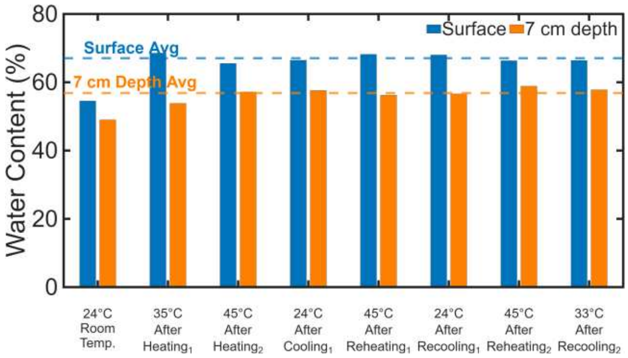

Figure 10. Traditional gravimetric water content during heating-cooling cycles.

Undrained shear strength profiles were obtained using T-bar penetration tests after each target temperature was obtained, as shown in Figure 11. In all cases, s_u increased with depth, reflecting the stress history and consolidation state of the soil specimen. The relatively high undrained shear strength measured at room temperature immediately after unloading is primarily attributed to negative pore water pressures generated during unloading. The subsequent introduction of surface water increased the water content (Figure 10) and likely led to some dissipation of suction as swelling of the clay was permitted. The reduction in undrained shear strength observed upon heating from room temperature (24 °C) to 35 °C reflects the combined influence of suction dissipation and thermal pressurization. During subsequent cooling, only partial recovery of s_u was observed. This incomplete recovery indicates that the strength loss induced during heating was not fully reversible and cannot be explained solely by transient pore pressure effects. Instead, the response is consistent with thermomechanical softening, whereby thermal loading modifies the soil fabric, leading to a permanent reduction in shear resistance.

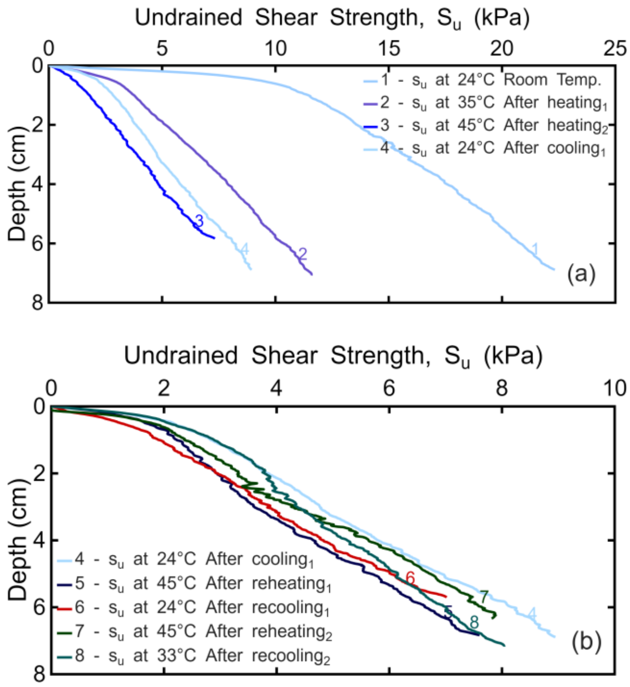

Figure 11. S_u profiles with heating-cooling cycles (a) initial profiles (b) repeated cycle profiles.

Reheating resulted in further reductions in s_u, indicating cumulative degradation of shear strength with repeated thermal cycling. Partial strength recovery during recooling reflects the reversible component associated with pore pressure dissipation, while the remaining strength loss is attributed to irreversible fabric alteration. Unlike earlier cycles, the final reheating stage (reheating$_2$) showed an overall increase in s_u, while recooling$_2$ produced strength gains in the upper soil and reductions at greater depths (Figure 11b). It is noted, however, that the measurements obtained during reheating$_2$ and recooling$_2$ may not fully represent the intrinsic strength response of the soil. At this stage, After multiple T-bar penetrations, the available undisturbed surface area became limited, and the reduced spacing between adjacent holes may have caused boundary effects during subsequent tests. Consequently, the shear strength measured in later stages i.e., 7th and 8th profile may reflect accumulated penetration-induced disturbance rather than the true undisturbed soil response and should be interpreted with caution. In contrast, earlier thermal cycles provided reliabe evidence of irreversible strength loss caused solely by elevated temperature.

4 CONCLUSIONS

The succesful development of a climate-controlled experimental chamber capable of independently regulating temperature and RH is presented. Stable environmental control was achieved using tuned PID feedback systems, enabling reproducible testing of saturated clay in changing environmental conditions. Heating induced a clear reduction in undrained shear strength, with partial recovery upon cooling but with evidence of irreversible strength loss attributed to thermomechanical softening. The integrated control and instrumentation framework provides insight into isolating thermal effects from moisture-driven changes. These results demonstrate the sensitivity of fine-grained soils to thermal loading and confirm the capability of the proposed system for investigating coupled thermo-mechanical behavior, providing a robust foundation for future centrifuge studies under controlled climatic conditions.

ACKNOWLEDGEMENTS

This work was supported by the National Science Foundation under Award No. 2332068. The views expressed are those of the authors and do not necessarily reflect those of the National Science Foundation.

REFERENCES

Archer, A., & Ng, C. W. W. (2018). Effects of temperature and relative humidity on a clay embankment: centrifuge modelling. *Géotechnique Letters*, *8*(2), 138–143. https://doi.org/10.1680/jgele.18.00002

Cao, J., Audibert, J. M. E., Al-Khafaji, Z., Phillips, R., & Popescu, R. (2002). Penetration Resistance of Suction Caissons in Clay . *In ISOPE International Ocean and Polar Engineering Conference (Pp. ISOPE-I). ISOPE.*, 800–806.

Castiblanco, P. M., Lozada, c., Caicedo, B., & Thorel, L. (2016). A new Climatic Chamber adapted to the mini-centrifuge for simulating Soil Drying. *EUROFUGE 2016, 3rd European Conference on Physical Modelling in Geotechnics.*, 111.

François, B., & Laloui, L. (2008). ACMEG-TS: A constitutive model for unsaturated soils under non-isothermal conditions. *International Journal for Numerical and Analytical Methods in Geomechanics*, *32*(16), 1955–1988. https://doi.org/10.1002/nag.712

Hudacsek, P., Bransby, M. F., Hallett, P. D., & Bengough, A. G. (2009). Centrifuge modelling of climatic effects on clay embankments. *Proceedings of the Institution of Civil Engineers - Engineering Sustainability*, *162*(2), 91–100. https://doi.org/10.1680/ensu.2009.162.2.91

Hueckel, T., & Borsetto, M. (1990). Thermoplasticity of Saturated Soils and Shales: Constitutive Equations. *Journal of Geotechnical Engineering*, *116*(12), 1765–1777. https://doi.org/10.1061/(ASCE)0733-9410(1990)116:12(1765)

Matziaris, V., Marshall, A. M., & Yu, H.-S. (2015). *Centrifuge Model Tests of Rainfall-Induced Landslides* (pp. 73–83). https://doi.org/10.1007/978-3-319-11053-0_7

Moncada, A., Damians, I. P., Olivella, S., & Bathurst, R. J. (2024). Thermo-hydraulic numerical modelling of in-soil conditions in reinforced soil walls. *Geosynthetics International*, *31*(6), 808–823. https://doi.org/10.1680/jgein.23.00026

Ng, C. W. W., Wang, Y., Zhang, S., & Zhang, Q. (2024). Effects of climate change on soil embankments for transport infrastructure. *Transportation Geotechnics*, *48*, 101324. https://doi.org/10.1016/j.trgeo.2024.101324

Pritchard, O. G., Hallett, S. H., & Farewell, T. S. (2014). Soil impacts on UK infrastructure: current and future climate. *Proceedings of the Institution of Civil Engineers - Engineering Sustainability*, *167*(4), 170–184. https://doi.org/10.1680/ensu.13.00035

Robinet, J.-C., Rahbaoui, A., Plas, F., & Lebon, P. (1996). A constitutive thermomechanical model for saturated clays. *Engineering Geology*, *41*(1–4), 145–169. https://doi.org/10.1016/0013-7952(95)00049-6

Sheob, M., Aldawood, S., & Madabhushi, S. S. C. (2026). Experimentally Studying the Thermal Sensitivity and Mechanical Response of Kaolin Clay due to Climatic Warming. *Geo-Congress 2026*.

Sheob, M., & Madabhushi, S. S. C. (2026). Thermomechanical Strength Changes in Saturated Clays: Pore Pressure and Fabric Effects. *(Submitted)*.

Shibasaki, T., Matsuura, S., & Hasegawa, Y. (2017). Temperature-dependent residual shear strength characteristics of smectite-bearing landslide soils. *Journal of Geophysical Research: Solid Earth*, *122*(2), 1449–1469. https://doi.org/10.1002/2016JB013241

Take, W. A., & Bolton, M. D. (2002). An atmospheric chamber for the investigation of the effect of seasonal moisture changes on clay slopes. *Physical Modelling in Geotechnics.*, 765–770.

Tristancho, J., Caicedo, B., Thorel, L., & Obregón, N. (2012). Climatic Chamber With Centrifuge to Simulate Different Weather Conditions. *Geotechnical Testing Journal*, *35*(1), 159–171. https://doi.org/10.1520/GTJ103620

Wang, Y., Zhang, Q., Zhang, S., Zhong, H., & Ng, C. W. W. (2025). Investigation of temperature effects on slope serviceability and subsequent rainfall-induced instability: a comparative centrifuge study. *Acta Geotechnica*, *20*(8), 4199–4212. https://doi.org/10.1007/s11440-025-02636-5